Published in final edited form as:
Neuroimage. 2012 February 01; 59(3): 2208–16. doi:10.1016/j.neuroimage.2011.09.086.

The influence of complex white matter architecture on the mean diffusivity in diffusion tensor MRI of the human brain

Sjoerd B. Vos[1,*], **Derek K. Jones**[2,3], **Ben Jeurissen**[4], **Max A. Viergever**[1], **Alexander Leemans**[1]

[1]Image Sciences Institute, University Medical Center Utrecht, Utrecht, the Netherlands

[2]CUBRIC, Cardiff University Brain Research Imaging Centre, School of Psychology, Cardiff University, Cardiff, United Kingdom

[3]Neuroscience and Mental Health Research Institute, Cardiff University, Cardiff, United Kingdom

[4]IBBT-VisionLab, University of Antwerp, Belgium

Abstract

In diffusion tensor magnetic resonance imaging (DT-MRI), limitations concerning complex fiber architecture (when an image voxel contains fiber populations with more than one dominant orientation) are well-known. Fractional anisotropy (FA) values are lower in such areas because of a lower directionality of diffusion on the voxel-scale, which makes the interpretation of FA less straightforward. Moreover, the interpretation of the axial and radial diffusivities is far from trivial when there is more than one dominant fiber orientation within a voxel. In this work, using (i) theoretical considerations, (ii) simulations, and (iii) experimental data, it is demonstrated that the mean diffusivity (or the trace of the diffusion tensor) is lower in complex white matter configurations, compared with tissue where there is a single dominant fiber orientation within the voxel. We show that the magnitude of this reduction depends on various factors, including configurational and microstructural properties (e.g., the relative contributions of different fiber populations) and acquisition settings (e.g., the b-value). These results increase our understanding of the quantitative metrics obtained from DT-MRI and, in particular, the effect of the microstructural architecture on the mean diffusivity. More importantly, they reinforce the growing awareness that differences in DT-MRI metrics need to be interpreted cautiously.

Keywords

diffusion tensor MRI; crossing fibers; complex fiber architecture; trace; mean diffusivity

1 Introduction

Many diffusion tensor MRI (DT-MRI) studies aim to determine whether differences in white matter (WM) microstructure can be observed between different groups of subjects, e.g.,

[*]Corresponding author: Sjoerd B. Vos, Image Sciences Institute, University Medical Center Utrecht Room Q.S.459, P.O. Box 85500, 3508 GA, Utrecht, the Netherlands, sjoerd@isi.uu.nl, +31 88 755 8562.
http://www.isi.uu.nl/People/?sjoerd

Europe PMC Funders Author Manuscripts

between healthy and diseased subjects, or to correlate some aspect of behaviour/performance with WM structural attributes. The two most frequently used metrics for characterizing tissue microstructure are the fractional anisotropy (FA) and the mean diffusivity (MD, which is defined as one third of the trace, Tr), which can be calculated from the diffusion tensor model (Basser et al., 1994; Jones, 2010; Tournier et al., 2011). Although DT-MRI is still the most widely used approach to analyze diffusion MRI data, there are many confounding factors that may affect the analyses and interpretation (e.g., Jones and Cercignani, 2010; Vos et al., 2011). One of the most important confounds is the inability of the tensor model to describe the diffusion correctly in regions of complex fiber architecture (e.g., bending or interdigitating fibers) (Basser et al., 2000; Frank, 2001; Alexander et al., 2002; Jones, 2003; Tuch, 2004). The FA, in particular, is known to be strongly affected in areas of complex fiber architecture, as described in detail in previous studies (Pierpaoli et al., 1996; Alexander et al., 2001; Tuch et al., 2003).

In this work, we will use the generic phrase of “crossing fibers” (abbreviated forthwith as “CF”) for any WM configuration where there is more than one dominant fiber orientation within a voxel, including crossing, “kissing”, twisting, splaying, kinking and bending configurations. By contrast, configurations where there is only one dominant fiber orientation will be referred to as “single fiber” configurations, and abbreviated forthwith as “SF”.

Recently, the interpretation of two other DT-MRI metrics, the axial and radial diffusivities (AD, the largest eigenvalue of the tensor; and RD, the average of the second and third eigenvalues of the tensor) was shown to be non-trivial in CF-configurations (Wheeler-Kingshott and Cercignani, 2009). Upon simulating a voxel with two crossing fiber populations and fitting a single tensor to that signal, increases in the AD of this tensor were observed when the RD of one of the underlying populations was increased. Similarly, decreases in the RD of such a CF-configuration were found when reducing the AD of one underlying population.

In this work, we expand upon previous simulations that show that the trace is influenced by the architectural configuration of the WM (Alexander et al., 2001). Many issues concerning this dependence are still unclear, such as the effect of the exact architectural configuration and whether the dependence can actually be observed in experimental data. Based on (i) a mathematical derivation of the trace of an ensemble of fiber populations, (ii) simulations, and (iii) experimental data, we demonstrate that the mean diffusivity is lower in CF-configurations compared to SF-configurations. We also show that the magnitude of this reduction depends on several factors that include microstructural and configurational properties (e.g., the intrinsic diffusivities of the fiber populations) and acquisition parameters (such as the b-value). These findings improve our understanding of quantitative DT-MRI indices and, in particular, show how architectural aspects and configurational properties of complex WM diffusion profiles can affect the estimation of the mean diffusivity.

2 Theory

In this section, a general mathematical formulation is given for the trace in a CF-configuration, in relation to the diffusion properties of the individual fiber populations. To simplify the mathematical expressions, we provide this derivation for the trace of the diffusion tensor, being equivalent to three times the MD. Using an extension of the Stejskal-Tanner equation (Stejskal and Tanner, 1965) to describe a diffusion signal originating from more than one fiber population (Alexander et al., 2001; Frank, 2001; Assaf et al., 2002), we find a lower trace in CF-configurations with respect to SF-configurations.

Consider the Stejskal-Tanner equation for a diffusion-weighted signal $S_{\mathbf{g}}$ along diffusion weighting direction **g** (Stejskal and Tanner, 1965):

$$S_{\mathbf{g}} = S_0 e^{-b\mathbf{g}^T \mathbf{D}\,\mathbf{g}} = S_0 e^{-b\,D_{\mathbf{g}}}, \tag{1}$$

where S_0 is the signal without diffusion weighting, b is the scalar value of diffusion weighting, **D** is the diffusion tensor, and D_{g} the apparent diffusion coefficient (ADC) along orientation **g**. Consequently, along a given gradient orientation **g**, the estimated diffusion coefficient D_{g} is:

$$D_{\mathbf{g}} = -\frac{1}{b}\ln\left(\frac{S_{\mathbf{g}}}{S_0}\right). \tag{2}$$

When multiple populations are present in one voxel, the signal originating from that voxel may be regarded as an average of the diffusion-weighted signals of the underlying fiber populations, if we assume that the spins of the different populations are in slow exchange (Alexander et al., 2001; Frank, 2001; Assaf et al., 2002). Eq. (1) can then be generalized to:

$$S_{\mathbf{g}} = S_0 \sum_{\alpha} f^{\alpha} e^{-b D_{\mathbf{g}}^{\alpha}}, \text{ with } \sum_{\alpha} f^{\alpha} = 1, \tag{3}$$

where $D_{\mathbf{g}}^{\alpha}$ represents the ADC of population α along orientation **g**, and f^{α} is the relative volume fraction of population α.

Combining Eqs. (2) and (3), one can calculate the estimated diffusivity in a CF-configuration along any direction **g**, denoted as $D_{\mathbf{g}}^{CF}$, as follows:

$$D_{\mathbf{g}}^{CF} = \frac{1}{b}\ln\left(\frac{1}{\sum_{\alpha} f^{\alpha} e^{-b D_{\mathbf{g}}^{\alpha}}}\right). \tag{4}$$

The trace is mathematically derived from the sum of the diffusivities along any three orthogonal orientations. These measurements can be taken along the orientations of the three eigenvectors of a specific population A, provided the diffusion profile is Gaussian or a low b-value ensures that the Gaussian part of the displacement profile dominates the signal

attenuation (Basser, 2002). By defining orientation $\mathbf{e}_1$ as the first eigenvector of population A, so that $D^A_{\mathbf{e}_1} = \lambda^A_1$, the diffusivity in a CF-configuration along this orientation (denoted as $D^{CF}_{\mathbf{e}_1}$) can be derived from Eq. (4) as:

$$\begin{aligned} D^{CF}_{\mathbf{e}_1} &= \frac{1}{b}\ln\left(\frac{1}{f^A e^{-b\lambda^A_1} + \sum_{\alpha\backslash A} f^\alpha e^{-bD^\alpha_{\mathbf{e}_1}}}\right) \\ &= \lambda^A_1 - F(b, f^A, f^\alpha, \mathbf{e}_1, \lambda^A_1), \end{aligned} \tag{5}$$

where

$$F(b, f^A, f^\alpha, \mathbf{g}, \lambda) = \frac{1}{b}\ln\left(f^A + \sum_{\alpha\backslash A} f^\alpha e^{-b\left(D^\alpha_{\mathbf{g}} - \lambda\right)}\right) \tag{6}$$

and the summation over $\alpha\backslash A$ indicates that this summation is over all populations α with the exception of population A.

Equivalently, $D^{CF}_{\mathbf{e}_2}$ and $D^{CF}_{\mathbf{e}_3}$, the diffusivities along $\mathbf{e}_2$ and $\mathbf{e}_3$ (the second and third eigenvectors of population A) can also be calculated with Eq. (5). By definition, the trace in a "crossing fibers" voxel, i.e., Tr($\mathbf{D}^{CF}$), can now be calculated as:

$$\begin{aligned} Tr(\mathbf{D}^{CF}) &= D^{CF}_{\mathbf{e}_1} + D^{CF}_{\mathbf{e}_2} + D^{CF}_{\mathbf{e}_3} \\ &= \lambda^A_1 + \lambda^A_2 + \lambda^A_3 - \sum_{i=1}^{3} F(b, f^A, f^\alpha, \mathbf{e}_i, \lambda^A_i) \\ &= Tr(\mathbf{D}^A) - \underbrace{\sum_{i=1}^{3} F(b, f^A, f^\alpha, \mathbf{e}_i, \lambda^A_i)}_{C}. \end{aligned} \tag{7}$$

Eq. (7) describes the trace after combining any number of fiber populations, in terms of the trace of population A and a correction factor C. This equation is valid for any set of relative volume fractions f^α and any geometric configuration of the fiber populations. From this general expression, it is trivial to derive a formulation for the trace for any specific fiber configuration. As an example, for an orthogonally oriented two-fiber population with equal volume fractions, Eq. (7) can be simplified to:

$$Tr(\mathbf{D}^{CF}) = Tr(\mathbf{D}^A) - \frac{1}{b}\ln\left(\frac{\left(2 + e^{b\left(\lambda^A_1 - \lambda^A_2\right)} + e^{-b\left(\lambda^A_1 - \lambda^A_2\right)}\right)}{4}\right), \tag{8}$$

when assuming equal diffusivity properties for each individual fiber population (i.e., $\lambda^A_1 = \lambda^B_1$, $\lambda^A_2 = \lambda^B_2$, and $\lambda^A_3 = \lambda^B_3$). As the anisotropy of the fiber populations decreases, i.e., as λ^A_1 and λ^A_2 differ less, the correction factor $\boldsymbol{C}$ will be smaller.

3 Materials and methods

3.1 Simulations

The mathematical framework presented in the previous section provides theoretical evidence for a change in trace for a voxel with more than one fiber population/orientation. In these calculations, however, several factors were not included that may influence the estimate of the trace, for example the choice of tensor estimation routine or the set of diffusion gradient sampling vectors. For a detailed characterization of these effects, simulation experiments were performed (Leemans et al., 2005).

To examine the influence of the angle between fibers in a CF-configuration, two identical fiber populations were defined (with FA = 0.7 and trace = 2.1×10^{-3} mm^2/s) (Le Bihan et al., 2001; Jones and Basser, 2004), in which one population (characterized by diffusion tensor D^A) was then rotated over a range of 0–90° with respect to the other population (characterized by diffusion tensor D^B). For each rotation, the diffusion-weighted signals along 60 gradient directions (b = 1000 s/mm^2) were computed for the resulting CF-configuration, assuming equal volume fractions (i.e., $f^A = f^B = 0.5$), according to Eq. (3). From this set of signals, a single tensor, D^{CF}, was estimated and the trace of that single tensor ($Tr(D^{CF})$) was compared with the trace of the underlying SF-populations ($Tr(D^{SF})$). This experiment was performed using three types of tensor estimation: (i) linear least squares, (ii) weighted linear least squares, and (iii) nonlinear least squares (initialized with the fitted values from a weighted linear least squares estimation) (Marquardt, 1963; Basser et al., 1994; Koay, 2010). For a more in-depth analysis, the eigenvalues of D^{CF} were compared to the eigenvalues of the individual diffusion tensors, D^{SF} (using only nonlinear least squares tensor estimation).

To determine the impact on the trace of changing the relative volume fractions of the individual fiber populations in an orthogonal crossing configuration, the volume fractions f^A and f^B (of populations A and B, respectively) were varied from 0 to 1, with $f^A + f^B = 1$ (while FA = 0.7, trace = 2.1×10^{-3} mm^2/s, b = 1000 s/mm^2, and with 60 unique diffusion encoding vectors). Again, $Tr(D^{CF})$ was calculated from D^{CF} estimated with the three different estimation procedures.

Furthermore, the impact of varying the relative orientations of three fiber populations on the trace was simulated, maintaining the same microstructural properties and acquisition properties as described above.

Previous work has shown that, in simulations of SF-voxels, there is variation in the estimated trace depending on the orientation of this population with respect to the diffusion encoding gradient set (Jones, 2004). This variation in trace decreased with increasing numbers of diffusion encoding directions, and the variation diminished at between 10–30 directions, depending on the FA of the simulated fiber population. Analogous to that work, we simulated two fiber populations crossing orthogonally with equal volume fractions using a range (6 to 60) of gradient directions (with b-value = 1000 s/mm^2 and the FA and trace values of the underlying fibers populations were 0.7 and 2.1×10^{-3} mm^2/s, respectively). For each number of gradient directions, the whole configuration of crossing populations

was rotated over the sphere in 2° steps around the azimuthal and polar axes (corresponding to over 4000 samples). After tensor estimation for each sample, the mean and standard deviation of $\mathrm{Tr}(\mathrm{D}^{CF})$ were calculated for each of the 6 to 60 gradient directions.

From Eq. (7) it becomes apparent that, apart from the configurational aspects, there are other factors that affect the trace values in CF-voxels, i.e., the FA and trace values of the individual fiber populations (FA^{SF} and $\mathrm{Tr}(\mathrm{D}^{SF})$, respectively), and the b-value. We have therefore simulated two fiber populations, crossing perpendicularly and with equal volume fractions, and varied FA^{SF}, $\mathrm{Tr}(\mathrm{D}^{SF})$ and the b-value in a range of relevant values. Since $\mathrm{Tr}(\mathrm{D}^{SF})$ is one of the parameters of interest in these simulations, the differences in $\mathrm{Tr}(\mathrm{D}^{CF})$ are shown relative to the simulated $\mathrm{Tr}(\mathrm{D}^{SF})$.

3.2 Data acquisition

Cardiac-gated DT-MRI datasets were acquired from six healthy subjects (3 males and 3 females) aged 23.7 to 29.1 years (mean age 26.1 years), on a 3T HDx MRI system (General Electric) using a single-shot spin echo EPI sequence with a b-value of 1200 s/mm^2, 60 gradient directions distributed uniformly over the half sphere (Jones et al., 1999), 6 b = 0 images and an ASSET factor 2. The acquisition matrix of 96×96 was reconstructed to 128×128 with a field-of-view of 230×230 mm^2, and 60 contiguous axial slices with thickness 2.4 mm were acquired, with an effective TR of 15 R–R intervals and a total acquisition time of approximately 25 min. In addition to the DT-MRI scans, 3D T1-weighted FSPGR scans were obtained with 1 mm isotropic resolution, using the following acquisition parameters: TR/TE/TI = 7.9/3.0/450 ms and a flip angle of 20°. All subjects gave a written informed consent to participate in this study under a protocol approved by the Cardiff University School of Psychology.

3.3 Pre-processing of experimental data

Prior to data analysis, each DT-MRI dataset was corrected for eddy current induced geometric distortions and subject motion by realigning all diffusion-weighted images (DWIs) to the b = 0 images using elastix (Klein et al., 2010), with an affine coregistration technique (with 12 degrees of freedom) and mutual information as the cost function (Pluim et al., 2003). In this procedure, the diffusion gradients were appropriately reoriented to account for subject motion (Leemans and Jones, 2009). The tensor model was fitted with the Levenberg-Marquardt nonlinear regression method (Marquardt, 1963), using the fitted values from a weighted linear least squares estimation as initialization.

3.4 Experimental data analysis

To characterize how complex fiber architecture affects the trace in experimental diffusion MRI data, we examined two WM fiber bundles that are known to have regions of complex fiber architecture, the cortico-spinal tracts (CST) and the arcuate fasciculus (AF) (Tuch et al., 2003; Behrens et al., 2007). These bundles were reconstructed with fiber tractography based on the estimated fiber orientation distribution obtained from constrained spherical deconvolution (CSD), in which spherical harmonics were limited to maximum harmonics of order $L = 8$ (Tournier et al., 2007; Jeurissen et al., 2011). For each bundle, all voxels that were intersected by the fiber tracts were used to investigate the impact of “crossing

fibers" on the trace. In addition, a WM segmentation was obtained from the T_1-weighted MR images using the Unified Segmentation algorithm (Ashburner and Friston, 2005) to examine the effect of complex fiber architecture on the trace in the global WM.

The linear and planar diffusion tensor geometry indices (Westin et al., 2002; Ennis and Kindlmann, 2006) were used as criteria to distinguish SF-voxels from CF-voxels. More specifically, all voxels where the planar diffusion coefficient (C_P) is largest – i.e., larger than the linear, C_L, and spherical, C_S, coefficients – were classified as CF-configuration voxels; all voxels where C_L was largest were classified as SF-configuration voxels; all voxels where C_S was largest were not included in the analyses, because a high C_S may not only arise from multiple fiber populations but also from partial voluming with cerebrospinal fluid. The average trace of the CF-regions ($Tr(D^{CF})$) and SF-regions ($Tr(D^{SF})$) was calculated for all subjects, and compared using the non-parametric Wilcoxon signed rank test. Image processing, tractography, and experimental analyses were performed in *ExploreDTI* (Leemans et al., 2009).

4 Results

4.1 Mathematical derivation of $Tr(D^{CF})$ values

From Eq. (7), the trace can be computed for a voxel with any number of fiber populations – once the FA and trace of each population has been specified, along with their volume fractions f^{α}, their geometric configuration and the b-value. As an example of a voxel with multiple fiber orientations, consider a voxel with one fiber bundle fanning out. To emulate such a voxel, Eq. (7) can be used to calculate the trace for any number of orientations. Assuming a set of in-plane orientations distributed uniformly along one quadrant of a circle (e.g., 0°, 45° and 90° for 3 populations, or 0°, 30°, 60° and 90° for 4 populations, etc.), one can observe an increase of the trace with more orientations, as shown in Fig. 1 (with FA^{SF} = 0.7, $Tr(D^{SF}) = 2.1 \times 10^{-3}$ mm^2/s, b-value = 1000 s/mm^2).

4.2 Simulations

In a voxel with two fiber populations, the trace in that voxel ($Tr(D^{CF})$) is not only dependent on the trace values of the underlying populations ($Tr(D^{SF})$), but also depends on the angle of intersection between these two fiber populations, as shown in Fig. 2a. With increases in the angle between the two populations, $Tr(D^{CF})$ gradually decreases with respect to $Tr(D^{SF})$, reaching its minimum when the populations are orthogonal, where $Tr(D^{CF})$ is 5% lower than $Tr(D^{SF})$. Performing this simulation for three different types of tensor estimation (linear, weighted linear, and nonlinear least squares) shows that the choice of tensor estimation during data analysis also influences the estimate of $Tr(D^{CF})$. The weighted linear least squares estimator consistently yields lower values of $Tr(D^{CF})$ than linear or nonlinear least squares estimation. The larger the decrease in trace, the bigger this difference between different tensor estimators becomes.

Fig. 2b illustrates that $Tr(D^{CF})$ also depends on the volume fractions of the two populations, with a minimum when both populations contribute equally (similar to the setting in Fig. 2a).

In addition, there is a small effect of the different tensor estimators on $Tr(D^{CF})$, with the weighted linear least squares estimation giving the lowest MD values.

To examine the reduction in $Tr(D^{CF})$ with larger angles between the individual populations in more detail, the eigenvalues ($\lambda_1 \geq \lambda_2 \geq \lambda_3 > 0$) of the tensor in a CF-configuration are investigated. Fig. 3 shows that λ_1 is lower in CF-voxels, with larger differences as the angle between the two individual populations increases. By contrast, λ_2 and λ_3 values are higher in CF-configurations than in SF-configurations.

In a CF-configuration with three fiber populations, the change in trace depends on the angles between all three populations (Fig. 4). Note that if the three populations are orthogonal, $Tr(D^{CF})$ is 6.5% lower than $Tr(D^{SF})$, lower than if there are only two orthogonal populations (Fig. 2).

The dependence of the mean and standard deviation of the trace values on the number of gradient directions is shown in Fig. 5. Independent of the number of gradient directions, $Tr(D^{CF})$ was consistently lower than $Tr(D^{SF})$. In the range of 10–30 gradient directions, the orientational dependence of the trace estimates is mostly reduced.

Fig. 6 shows that the b-value, as well as both microstructural parameters present in Eq. (7), FA^{SF} and $Tr(D^{SF})$, all modulate $Tr(D^{CF})$.

4.3 Experimental data

In experimental data, the trace in CF-voxels is significantly lower than in SF-voxels, confirming the results of the simulations. For all subjects, $Tr(D^{CF})$ is lower than $Tr(D^{SF})$ in the CST, AF, and the total WM (Table 1). Fig. 7 illustrates the regions of linear and planar diffusion along the CST and AF. In Fig. 8, it can be seen that this differentiation between regions of linear and planar diffusion is also consistent across subjects within the WM.

5 Discussion

In DT-MRI, the issue of “crossing fibers” is well-known. Apart from a single study showing that the trace is affected in simulated fiber crossings (Alexander et al., 2001), no research has been conducted to validate this finding *in vivo*. In this work, we have studied this observation in further detail, starting from a general theoretical basis that can explain these results. In addition, simulations have been performed to highlight the effect of several aspects related to “crossing fibers”. Finally, to the best of our knowledge, we have demonstrated for the first time that the expected reduction in trace in complex WM tissue can also be shown in real diffusion MRI data.

5.1 Mathematical derivation of $Tr(D^{CF})$ values

The mathematical correction factor derived in this work (Eqs. (7) and (8)) shows that the trace in a CF-voxel is not always equal to the trace in an SF-voxel. For two orthogonal populations, it can be deduced from Eq. (8) that $Tr(D^{CF}) \leq Tr(D^{SF})$ will always hold. The fraction in the logarithm in Eq. (8) will never be smaller than one, so the correction factor to the $Tr(D^{SF})$, C, will always be equal to or larger than zero.

5.2 Simulations

Following the mathematical derivation demonstrating a decrease in trace in "crossing fibers", results from simulation experiments support a reduction in trace in voxels with complex fiber architecture. Moreover, this decrease depends on the configuration of the crossing, i.e., the angle of intersection between the populations and the volume fraction of each of the fiber populations in a voxel (Fig. 2). It is apparent from Eq. (7) that the number, orientation, FA, and trace of the individual populations, and the b-value affect $\mathrm{Tr}(\mathrm{D}^{CF})$. In simulations, all these configurational (Figs. 2 and 4), microstructural (Fig. 6a, b) and acquisition (Fig. 6c) parameters are confirmed to modulate $\mathrm{Tr}(\mathrm{D}^{CF})$. Note that the relative change in $\mathrm{Tr}(\mathrm{D}^{CF})$ with all these parameters is nonlinear.

Variability in the estimated tensor depending on the chosen tensor estimation method has been described previously by Jones and Basser (2004) (see also Jones and Cercignani, 2010). To examine the effect of various tensor fitting procedures on the results presented in this work, the effects of changing the angle between two populations and the volume fractions of these populations have been investigated with three types of tensor estimation. From Fig. 2 we can see that the weighted least squares systematically yields lower trace estimates in CF-configurations than linear and nonlinear tensor estimation. These simulations were noise-free, so comparable results for the linear and nonlinear estimators were expected (Jones and Basser, 2004). The lower trace estimates from the weighted least squares algorithm can be explained by the fact that this estimator weights each diffusion measurement as a function of its signal magnitude. Given that the highest signals are obtained in directions with lowest diffusion, the estimator gives greater weights to low diffusion measurements, yielding a lower trace estimate.

5.2.1 Eigenvalue simulations—With lower MD values in regions of complex fiber architecture, an associated reduction in one or more of the tensor's eigenvalues ($\lambda_1 \geq \lambda_2 \geq \lambda_3 > 0$) would be expected. With two fiber populations in a voxel, the diffusivity will become more planar, which would intuitively lead to an underestimation of λ_1 and an overestimation of λ_2. These expected changes are confirmed for λ_1 and λ_2, as shown in Fig. 3. The increase in λ_3 (Fig. 3), on the other hand, is counterintuitive. The third eigenvector of the CF-configuration is oriented perpendicular to the plane of the crossing. In the simulations, both individual tensors were defined to be axially symmetric, which results in equal diffusivities perpendicular to their crossing. As a result, theory dictates that λ_3 would not be affected in such a "fiber crossing". In the simulations, however, λ_3 is slightly overestimated. This overestimation of λ_3 originates from the finite number of sampling directions in data acquisition protocols: in a two-fiber crossing, λ_3 will only be the same as in a "single fiber" population when sampled precisely perpendicularly to the plane of the crossing.

5.2.2 Number of gradient directions—Until now, only one study has previously shown that, in simulations, the trace is underestimated in CF-configurations (Alexander et al., 2001). When simulating a crossing between two fiber populations with two different sets of six gradient directions, Alexander et al. (2001) observed trace values that were lower than the simulated trace values of the individual constituent fiber populations. However,

the decrease in trace that was observed with the two sets of gradient orientations varied drastically. More recently, it was shown in simulations that in SF-voxels, variation in the estimated trace was observed depending on the orientation of this population with respect to the diffusion encoding gradient set (Jones, 2004). This variation in trace decreased as the number of gradient encoding directions was increased, with the variation diminished at between 10–30 directions, depending on the FA of the simulated fiber population. To confirm that the observed reduction in trace seen in the simulations carried out by Alexander et al. (2001) was not due to the relatively low number of gradient directions, we have investigated whether such variations in trace values are also present in CF-voxels. As shown in Fig. 5, $Tr(D^{CF})$ was consistently lower than $Tr(D^{SF})$ for all number of gradient directions. In agreement with the findings for SF-configurations (Jones, 2004), the orientational dependence of the trace estimates is largely reduced in the range of 10–30 unique gradient directions.

5.3 Experimental data analysis

Previous studies have shown that in experimental data, MD values can differ between fiber bundles (e.g., Eluvathingal et al., 2007; Lebel et al., 2008). Even within one bundle, however, there can already be a large heterogeneity of MD values (Jones et al., 2005). In this work, we show such heterogeneity, and, more specifically, we demonstrate that MD values in CF-configurations are significantly lower than in SF-configurations (Table 1, Fig. 9). This difference, observed in the two bundles of interest, the CST and the AF, is also valid for the global WM (Table 1).

It can be observed from Table 1 that while $Tr(D^{SF})$ values are not different for the CST and the AF, the mean $Tr(D^{CF})$ values are lower in the CST than in the AF for all subjects. For the CST, $Tr(D^{CF})$ is 8% lower than $Tr(D^{SF})$, whereas this decrease is only 3% for the AF. This variation may be attributed to a difference in configurational properties between the two bundles. Other WM bundles crossing the CST may be more orthogonally oriented to the CST than is the case for bundles intersecting the AF, which could explain the larger decrease in $Tr(D^{CF})$ in the CST than in the AF (as is illustrated in Fig. 2a). In addition, there could be a larger portion of equally distributed volume fractions in the CST compared to the AF, which could also contribute to lower $Tr(D^{CF})$ values in the CST than in the AF (Fig. 2b).

The dependence of the MD on the tissue geometry has implications for statistical testing. In regions that are comprised of voxels with purely SF-configurations, the MD will be relatively uniform. Likewise, for areas of tissue where there is a uniformity in the complexity of the tissue, the MD may be lower – but it will be uniformly lower. However, in regions that contain a mixture of SF- and CF-configurations, or CF-configurations that take different geometrical forms, there will be a larger variation in MD. Consequently, there will be a higher variance in such regions, and therefore less statistical power to detect differences in the MD.

In some neuropathological studies, investigating Wallerian degeneration and mild cognitive impairment, higher FA values were observed in patients than in healthy controls (Pierpaoli et al., 2001; Douaud et al., 2011). In any CF-configuration, degeneration of one fiber bundle could cause the other fiber bundle to become more dominant, resulting in an increase in FA.

Similarly, such a physiological change could cause an increase in MD, which, in the context of our findings, may not be indicative for a change in MD of one of the underlying fiber bundles.

In recent years, “crossing fibers” has been one of the foci of diffusion MRI research, resulting in alternative methods that aim to describe the estimated diffusion more accurately in regions of complex fiber architecture, such as CSD, Q-ball Imaging, diffusion spectrum imaging, the ball-and-multiple-sticks model, or multi-tensor modeling (Tuch et al., 2002; Tuch, 2004; Behrens et al., 2007; Tournier et al., 2007; Wedeen et al., 2008). Fiber tractography based on these new techniques can resolve complex fiber architecture more accurately, even in regions with three fiber populations, e.g., the intersection of the CST, superior longitudinal fasciculus, and lateral projections of the corpus callosum (Descoteaux et al., 2009; Fillard et al., 2011; Jeurissen et al., 2011). When using such techniques to obtain fiber tract segmentations for analyses of the underlying DT-MRI metrics (Zarei et al., 2009), the amount of CF-voxels is increased (since tracking can continue through complex fiber architecture where tensor-based tracking would terminate). As a result, the average MD for the whole bundle may be affected more than when tensor-based tractography algorithms are used for tract segmentations, an effect that may need to be considered during data analysis.

To estimate the MD of individual fiber populations in voxels with complex fiber architecture, one could opt to model the diffusion signal using multiple tensors (Tuch et al., 2002). Multi-tensor tractography aims to model two or three tensors per voxel, propagating the fiber tract by selecting the tensor with its direction most consistent with the tract (Peled et al., 2006). For each tract, the MD of the tensor chosen by the tractography algorithm could be used to calculate bundle-specific diffusion measures, dubbed “tensor selection”. Ideally, this yields more accurate estimates of the MD for that specific bundle (and, similarly, also for other DT-MRI metrics). Current two-tensor methods estimate all three eigenvalues of both tensors (assuming prolate tensors), and can thus be used for this “tensor selection” methodology (Rathi et al., 2010). However, the most recent estimates on the amount of WM voxels with CF-configurations show that roughly 30 to 40% of all WM voxels contain three or more populations (Jeurissen et al., 2010), indicating that two-tensor models may be inadequate for modeling the underlying diffusion signals in these regions. Furthermore, multiple-tensor models may not provide unique solutions for each of the underlying fiber populations, which further complicates data interpretation.

In conclusion, we have provided a theoretical framework and concomitant simulations demonstrating a reduced MD in complex WM configurations. For the first time, this reduction is observed in experimental data (e.g., the CST and the AF). These results improve our understanding of quantitative indices derived from DT-MRI in areas of “crossing fibers” and the impact of numerous factors, including configurational and microstructural properties (e.g., the relative contributions of different fiber populations) and acquisition settings (e.g., the b-value). Most importantly, our findings strengthen the increasing awareness that DT-MRI metrics need to be interpreted with care, and that it is essential to characterize the effects of complex fiber architecture on the MD in order to improve the specificity of observed MD changes *in vivo*.

Acknowledgments

This work was financially supported by the project Care4Me (Cooperative Advanced REsearch for Medical Efficiency) in the framework of the EU research programme ITEA (Information Technology for European Advancement) and the CONNECT Consortium, supported by Framework 7 of the European Commission (Future and Emerging Technologies programme). The authors would like to thank Dr. John Evans, Chief Physicist of CUBRIC, for assistance in acquiring the MR data.

References

Alexander AL, Hasan KM, Lazar M, Tsuruda JS, Parker DL. Analysis of partial volume effects in Diffusion-Tensor MRI. Magnetic Resonance in Medicine. 2001; 45 (5) 770–780. [PubMed: 11323803]

Alexander DC, Barker GJ, Arridge SR. Detection and modeling of non-Gaussian apparent diffusion coefficient profiles in human brain data. Magnetic Resonance in Medicine. 2002; 48 (2) 331–340. [PubMed: 12210942]

Ashburner J, Friston KJ. Unified segmentation. NeuroImage. 2005; 26 (3) 839–851. [PubMed: 15955494]

Assaf Y, Ben-Bashat D, Chapman J, Peled S, Biton I, Kafri M, Segev Y, Hendler T, Korczyn A, Graif M, Cohen Y. High b-value q-space analyzed diffusion-weighted MRI: Application to multiple sclerosis. Magn Reson Med. 2002; 47 (1) 115–126. [PubMed: 11754450]

Basser PJ. Relationships between diffusion tensor and q-space MRI. Magnetic Resonance in Medicine. 2002; 47 (2) 392–397. [PubMed: 11810685]

Basser PJ, Mattiello J, LeBihan D. MR Diffusion Tensor Spectroscopy and Imaging. Biophysical Journal. 1994; Jan; 66 (1) 259–267. [PubMed: 8130344]

Basser PJ, Pajevic S, Pierpaoli C, Duda J, Aldroubi A. In vivo fiber tractography using DT-MRI data. Magnetic Resonance in Medicine. 2000; 44 (4) 625–632. [PubMed: 11025519]

Behrens T, Johansen-Berg H, Jbabdi S, Rushworth M, Woolrich M. Probabilistic diffusion tractography with multiple fibre orientations: What can we gain? NeuroImage. 2007; 34 (1) 144–155. [PubMed: 17070705]

Descoteaux M, Deriche R, Knosche TR, Anwander A. Deterministic and Probabilistic Tractography based on Complex Fibre Orientation Distributions. IEEE Transactions on Medical Imaging. 2009; February; 28 (2) 269–286. [PubMed: 19188114]

Douaud G, Jbabdi S, Behrens TE, Menke RA, Gass A, Monsch AU, Rao A, Whitcher B, Kindlmann G, Matthews PM, Smith S. DTI measures in crossing-fibre areas: Increased diffusion anisotropy reveals early white matter alteration in MCI and mild Alzheimer's disease. NeuroImage. 2011; April; 55 (2) 880–890. [PubMed: 21182970]

Eluvathingal TJ, Hasan KM, Kramer L, Fletcher JM, Ewing-Cobbs L. Quantitative Diffusion Tensor tractography of association and projection fibers in normally developing children and adolescents. Cereb Cortex. 2007; 17 (12) 2760–2768. [PubMed: 17307759]

Ennis DB, Kindlmann G. Orthogonal tensor invariants and the analysis of diffusion tensor magnetic resonance images. Magn Reson Med. 2006; 55 (1) 136–146. [PubMed: 16342267]

Fillard P, Descoteaux M, Goh A, Gouttard S, Jeurissen B, Malcolm J, Ramirez-Manzanares A, Reisert M, Sakaie K, Tensaouti F, Yo T, et al. Quantitative Evaluation of 10 Tractography Algorithms on a Realistic Diffusion MR Phantom. NeuroImage. 2011; May; 56 (1) 220–234. [PubMed: 21256221]

Frank LR. Anisotropy in High Angular Resolution Diffusion-Weighted MRI. Magnetic Resonance in Medicine. 2001; 45 (6) 935–939. [PubMed: 11378869]

Jeurissen B, Leemans A, Jones DK, Tournier J-D, Sijbers J. Probabilistic fiber tracking using the residual bootstrap with constrained spherical deconvolution. Human Brain Mapping. 2011; 32: 461–479. [PubMed: 21319270]

Jeurissen, B; Leemans, A; Tournier, J-D; Jones, DK; Sijbers, J. Estimating the number of fiber orientations in diffusion MRI voxels: a constrained spherical deconvolution study; Proceedings of the 18th Annual Meeting of International Society for Magnetic Resonance in Medicine; Stockholm, Sweden. 2010. 573

Jones DK. Determining and visualizing uncertainty in estimates of fiber orientation from Diffusion Tensor MRI. Magnetic Resonance in Medicine. 2003; 49 (1) 7–12. [PubMed: 12509814]

Jones DK. The effect of gradient sampling schemes on measures derived from Diffusion Tensor MRI: A Monte Carlo study. Magnetic Resonance in Medicine. 2004; 51 (4) 807–815. [PubMed: 15065255]

Jones DK. Precision and Accuracy in Diffusion Tensor Magnetic Resonance Imaging. Topics in Magnetic Resonance Imaging. 2010; April; 21 (2) 87–99. [PubMed: 21613874]

Jones DK, Basser PJ. Squashing peanuts and smashing pumpkins": How noise distorts diffusion-weighted MR data. Magnetic Resonance in Medicine. 2004; 52 (5) 979–993. [PubMed: 15508154]

Jones DK, Cercignani M. Twenty-five pitfalls in the analysis of diffusion MRI data. NMR Biomed. 2010; 23 (7) 803–820. [PubMed: 20886566]

Jones DK, Horsfield M, Simmons A. Optimal strategies for measuring diffusion in anisotropic systems by Magnetic Resonance Imaging. Magnetic Resonance in Medicine. 1999; 42 (3) 515–525. [PubMed: 10467296]

Jones DK, Travis AR, Eden G, Pierpaoli C, Basser PJ. PASTA: Pointwise assessment of streamline tractography attributes. Magnetic Resonance in Medicine. 2005; 53 (6) 1462–1467. [PubMed: 15906294]

Klein S, Staring M, Murphy K, Viergever MA, Pluim J. elastix: A Toolbox for Intensity-Based Medical Image Registration. IEEE Transactions on Medical Imaging. 2010; 29: 196–205. [PubMed: 19923044]

Koay, CG. Diffusion MRI: Theory, Methods and Applications. Oxford University Press; 2010.

Le Bihan D, Mangin J-F, Poupon C, Clark CA, Pappata S, Molko N, Chabriat H. Diffusion Tensor Imaging: Concepts and applications. Journal of Magnetic Resonance Imaging. 2001; 13 (4) 534–546. [PubMed: 11276097]

Lebel C, Walker L, Leemans A, Phillips L, Beaulieu C. Microstructural maturation of the human brain from childhood to adulthood. NeuroImage. 2008; 40 (3) 1044–1055. [PubMed: 18295509]

Leemans, A; Jeurissen, B; Sijbers, J; Jones, DK. ExploreDTI: a graphical toolbox for processing, analyzing, and visualizing diffusion MR data; Proceedings of the 17th Annual Meeting of International Society for Magnetic Resonance in Medicine; Hawaii, USA. 2009.

Leemans A, Jones DK. The B-matrix must be rotated when correcting for subject motion in DTI data. Magnetic Resonance in Medicine. 2009; 61 (6) 1336–1349. [PubMed: 19319973]

Leemans A, Sijbers J, Verhoye M, van der Linden A, van Dyck D. Mathematical framework for simulating Diffusion Tensor MR neural fiber bundles. Magnetic Resonance in Medicine. 2005; 53 (4) 944–953. [PubMed: 15799061]

Marquardt D. An Algorithm for Least-Squares Estimation of Nonlinear Parameters. Journal of the Society for Industrial and Applied Mathematics. 1963; 11: 431–441.

Peled S, Friman O, Jolesz F, Westin C-F. Geometrically constrained two-tensor model for crossing tracts in DWI. Magnetic Resonance Imaging. 2006; 24 (9) 1263–1270. [PubMed: 17071347]

Pierpaoli C, Barnett A, Pajevic S, Chen R, Penix L, Virta A, Basser PJ. Water Diffusion Changes in Wallerian Degeneration and Their Dependence on White Matter Architecture. NeuroImage. 2001; 13 (6) 1174–1185. [PubMed: 11352623]

Pierpaoli C, Jezzard P, Basser PJ, Barnett A, Di Chiro G. Diffusion Tensor MR Imaging of the human brain. Radiology. 1996; 201 (3) 637–648. [PubMed: 8939209]

Pluim JPW, Maintz JBA, Viergever MA. Mutual-information-based registration of medical images: a survey. IEEE Transactions on Medical Imaging. 2003; 22 (8) 986–1004. [PubMed: 12906253]

Rathi, Y; Malcolm, J; Michailovich, O; Goldstein, J; Seidman, L; McCarley, R; Westin, C-F; Shenton, ME. Biomarkers for Identifying First-Episode Schizophrenia Patients using Diffusion Weighted Imaging; Proceedings of the MICCAI, 2010; Beijing, China. 2010. 657–655.

Stejskal E, Tanner J. Spin diffusion measurements: spin echoes in the presence of a timedependent field gradient. The Journal of Chemical Physics. 1965; 42 (1) 288–292.

Tournier J-D, Calamante F, Connelly A. Robust determination of the fibre orientation distribution in diffusion MRI: Non-negativity constrained super-resolved spherical deconvolution. NeuroImage. 2007; 35 (4) 1459–1472. [PubMed: 17379540]

Tournier J-D, Mori S, Leemans A. Diffusion Tensor Imaging and Beyond. Magnetic Resonance in Medicine. 2011; June; 65 (6) 1532–1556. [PubMed: 21469191]

Tuch DS. Q-ball imaging. Magn Reson Med. 2004; 52 (6) 1358–1372. [PubMed: 15562495]

Tuch DS, Reese TG, Wiegell MR, Makris N, Belliveau JW, Wedeen VJ. High angular resolution diffusion imaging reveals intravoxel white matter fiber heterogeneity. Magnetic Resonance in Medicine. 2002; 48 (4) 577–582. [PubMed: 12353272]

Tuch DS, Reese TG, Wiegell MR, Wedeen VJ. Diffusion MRI of Complex Neural Architecture. Neuron. 2003; 40 (5) 885–895. [PubMed: 14659088]

Vos SB, Viergever MA, Jones DK, Leemans A. Partial volume effect as a hidden covariate in DTI analyses. NeuroImage. 2011; 55: 1566–1576. [PubMed: 21262366]

Wedeen V, Wang R, Schmahmann J, Benner T, Tseng W, Dai G, Pandya D, Hagmann P, D'Arceuil H, de Crespigny A. Diffusion spectrum magnetic resonance imaging (DSI) tractography of crossing fibers. NeuroImage. 2008; 41 (4) 1267–1277. [PubMed: 18495497]

Westin C-F, Maier SE, Mamata H, Nabavi A, Jolesz FA, Kikinis R. Processing and visualization for diffusion tensor MRI. Medical Image Analysis. 2002; 6 (2) 93–108. [PubMed: 12044998]

Wheeler-Kingshott CAM, Cercignani M. About "axial" and "radial" diffusivities. Magnetic Resonance in Medicine. 2009; 61 (5) 1255–1260. [PubMed: 19253405]

Zarei M, Damoiseaux JS, Morgese C, Beckmann CF, Smith SM, Matthews PM, Scheltens P, Rombouts SA, Barkhof F. Regional White Matter Integrity Differentiates Between Vascular Dementia and Alzheimer Disease. Stroke. 2009; 40 (3) 773–779. [PubMed: 19164789]

Europe PMC Funders Author Manuscripts

Europe PMC Funders Author Manuscripts

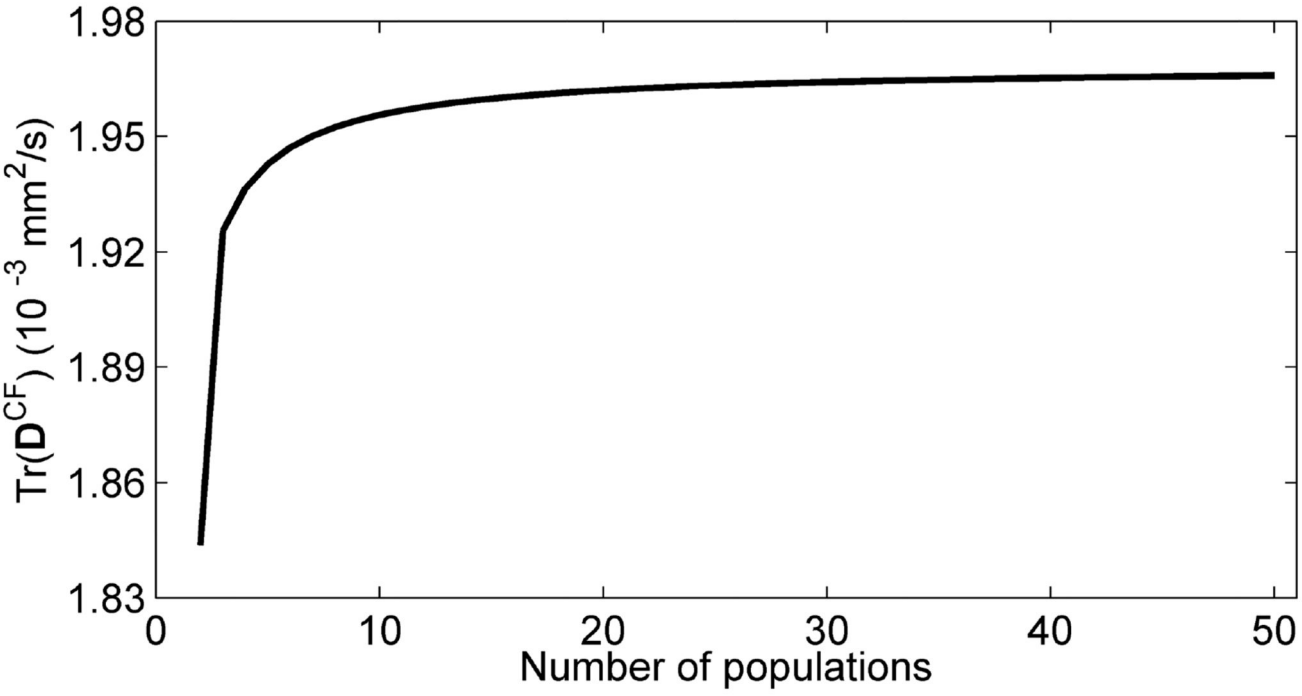

Figure 1.

The calculated trace in a "crossing fibers" voxel, $Tr(D^{CF})$, is shown for a crossing with a varying number of orientations in a plane. Such a configuration could be considered analogous to fibers fanning out in a voxel, as for instance can be found in the cortico-spinal tracts. Compared with the trace in a voxel with one fiber orientation ($Tr(D^{SF}) = 2.1 \times 10^{-3}$ mm^2/s), the $Tr(D^{CF})$ is strongly reduced for two orientations. With more orientations, $Tr(D^{CF})$ gradually increases, stabilizing in the range of 30–50 fiber orientations.

Europe PMC Funders Author Manuscripts

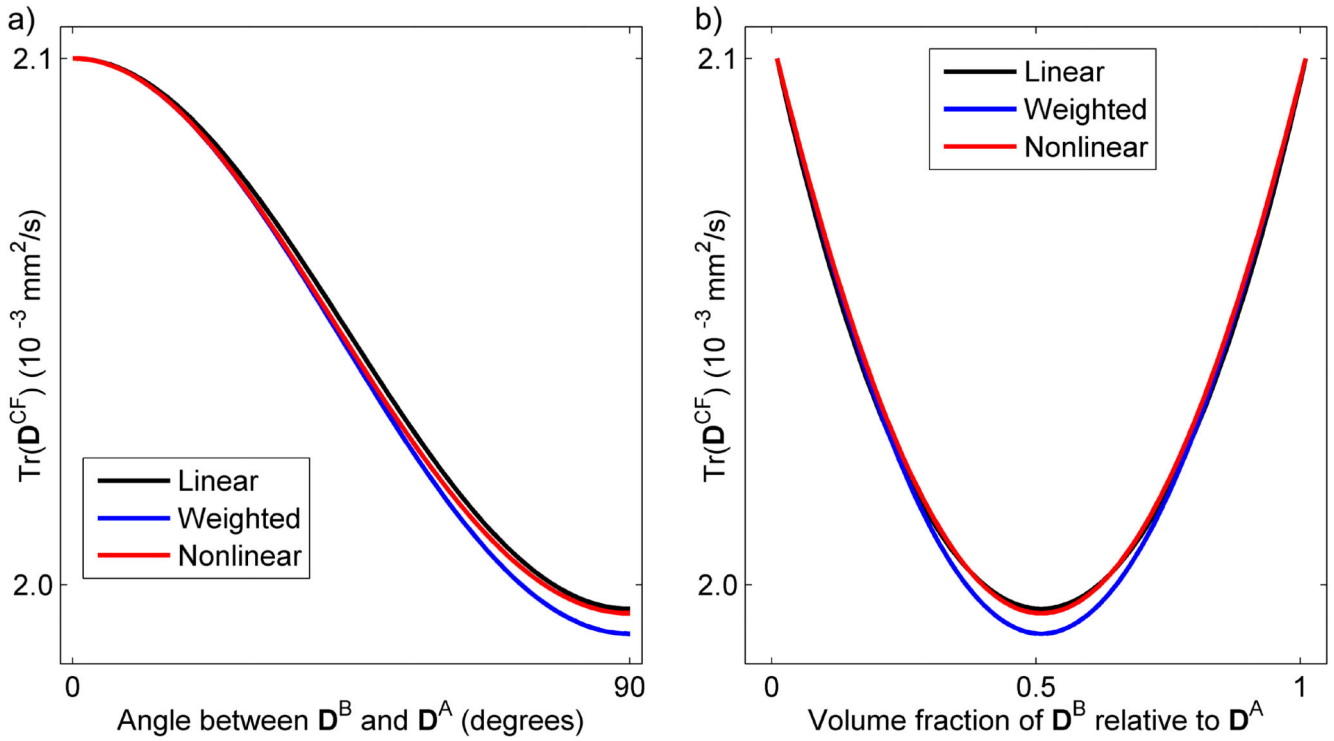

Figure 2.

(a) Increasing the angle of intersection between two fiber populations (D^A and D^B) up to 90° decreases the trace in a "crossing fibers" configurations, $Tr(D^{CF})$. Performing this simulation with three types of tensor estimation shows that the choice of tensor estimation also affects the trace (linear least squares estimation is illustrated in black, weighted least squares in blue, nonlinear least squares in red). (b) The volume fractions of the two populations in one voxel also modulates $Tr(D^{CF})$. As in (a), the type of tensor estimation also affects the trace in (b).

Europe PMC Funders Author Manuscripts

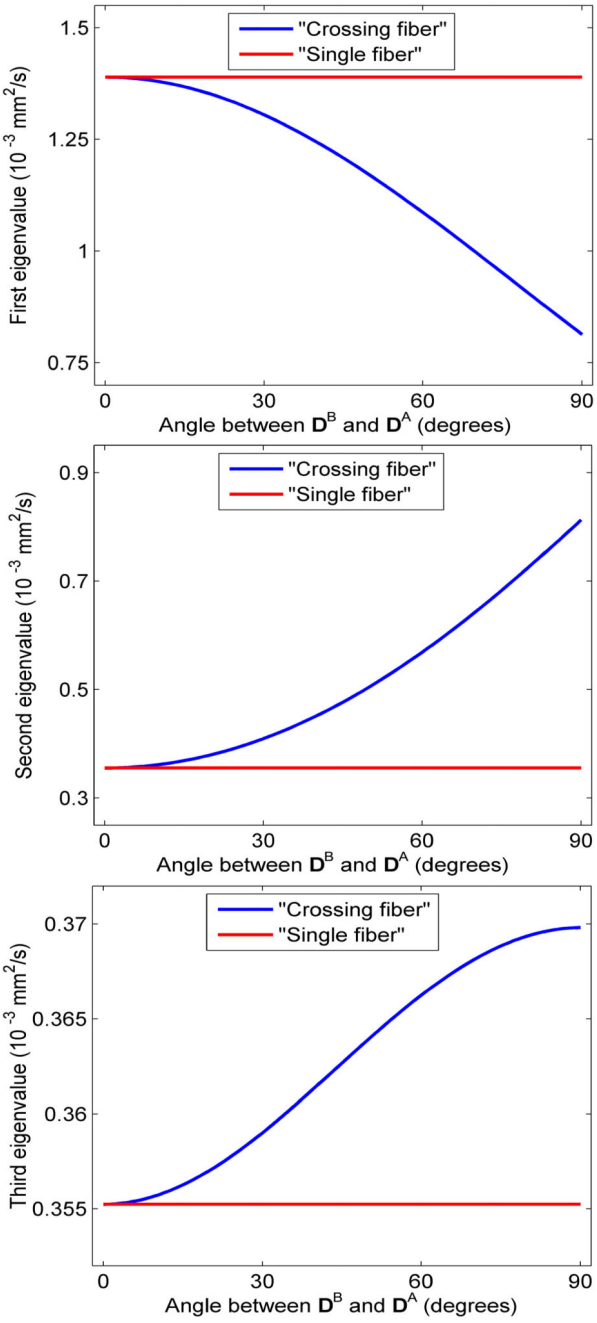

Figure 3.

Diffusivity profiles of the first, second, and third eigenvalues depending on the angle of intersection between the two fiber populations (D^A and D^B). The first eigenvalue is smaller in “crossing fibers” configurations than in “single fiber” configurations, whereas the second and third eigenvalues are larger.

Europe PMC Funders Author Manuscripts

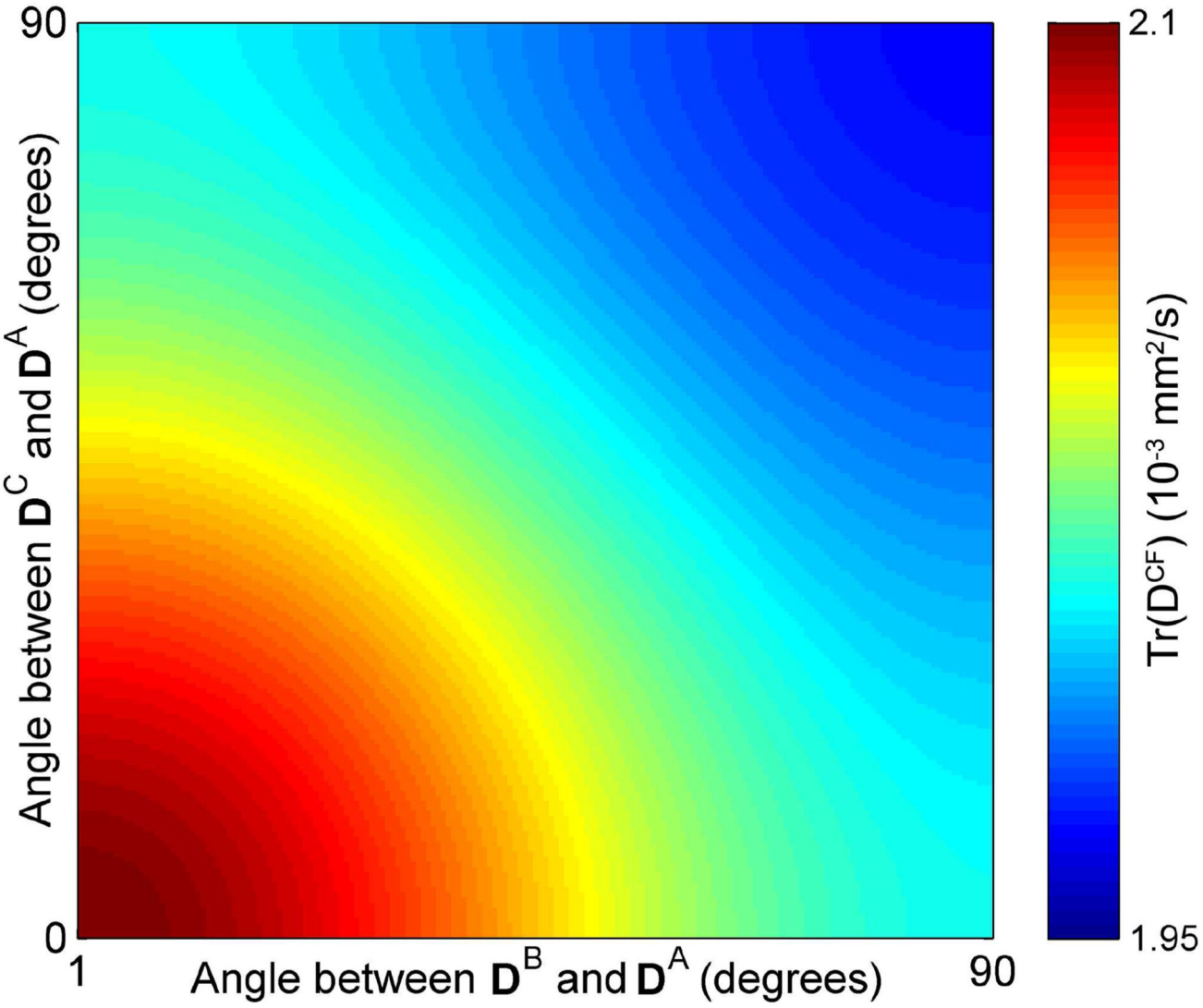

Figure 4.

When three fiber populations intersect, the trace (Tr(DC^F)) is affected by the angle of both the second (D^B) and third (DC) population with respect to the first population (D^A).

Europe PMC Funders Author Manuscripts

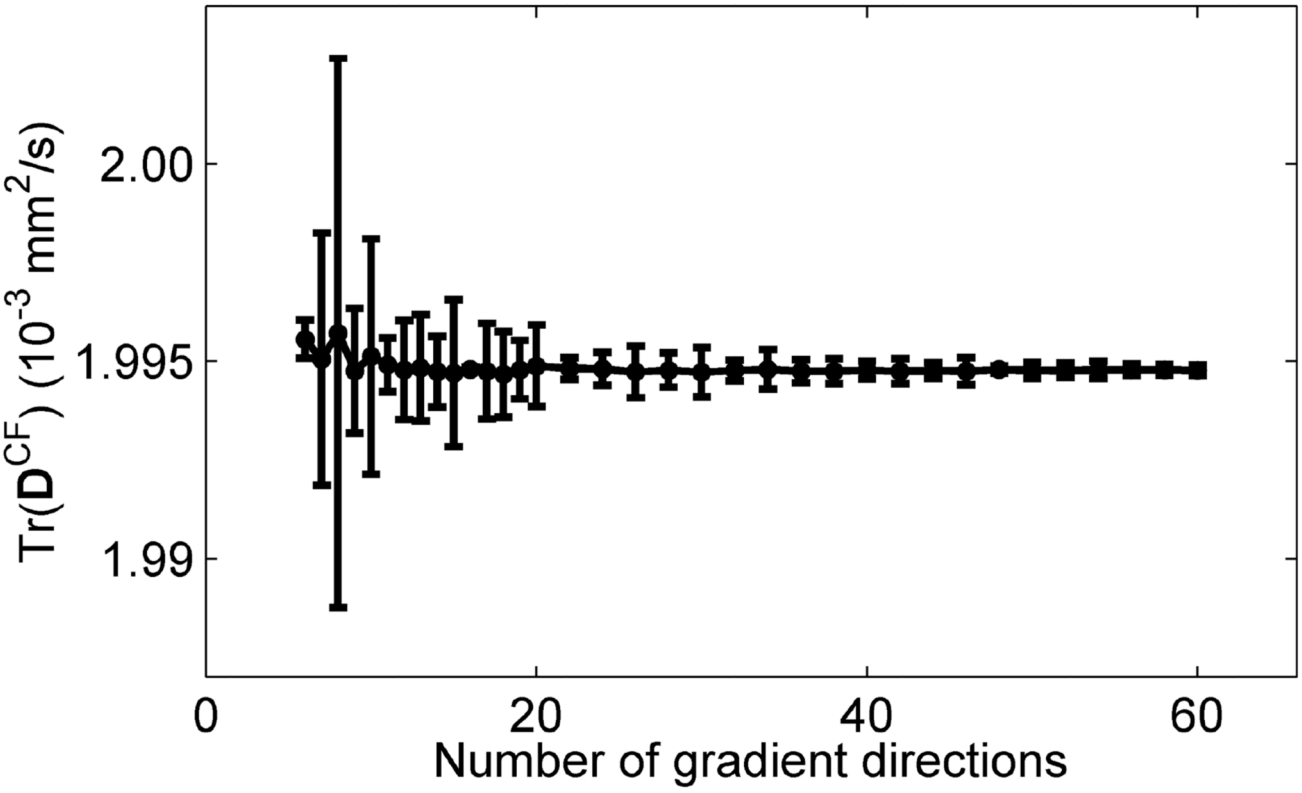

Figure 5.

Variation in the estimated trace in a "crossing fibers" configuration, $Tr(D^{CF})$, depending on the number of unique sampling directions for two populations crossing at 90°. The average $Tr(DC^{F})$ and standard deviation (error bars) have been calculated from over 4000 different orientations. $Tr(DC^{F})$ is lower than the trace in single fiber voxels ($Tr(D^{SF}) = 2.1\times10^{-3}$ mm^2/s) for all number of gradient directions.

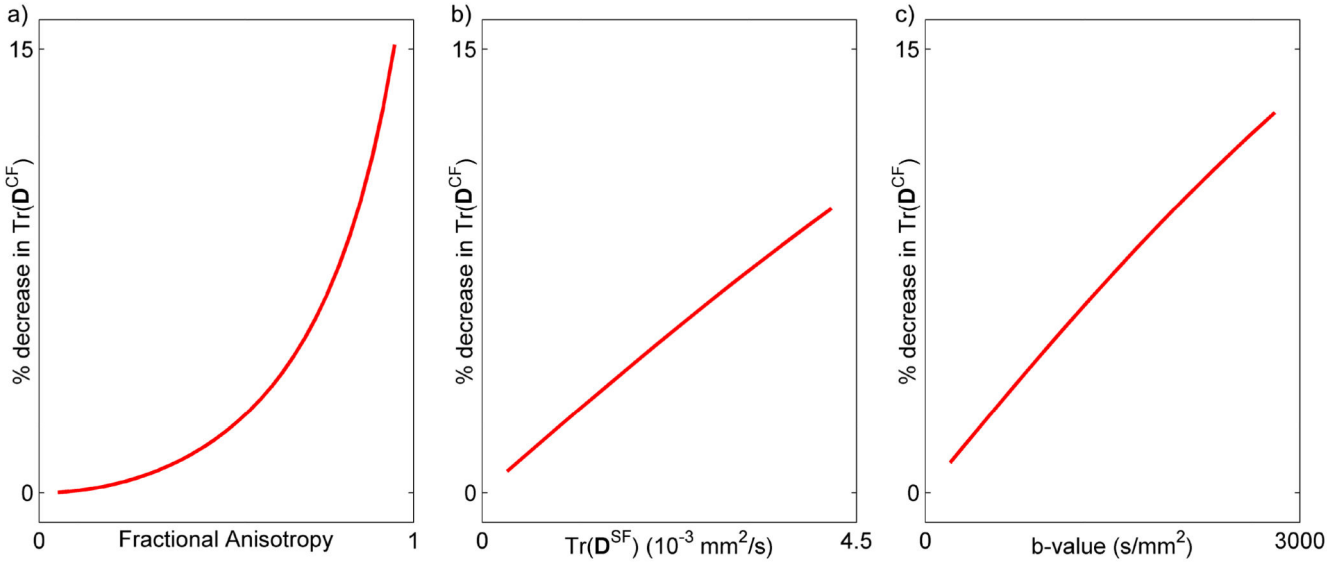

Figure 6.

The effect of simulation parameters (a: fractional anisotropy; b: trace of a "single fiber" population ($Tr(D^{SF})$); c: b-value) on the relative decrease in trace in a "crossing fibers" configuration, $Tr(D^{CF})$, with two orthogonally oriented fiber populations (with equal volume fractions).

Europe PMC Funders Author Manuscripts

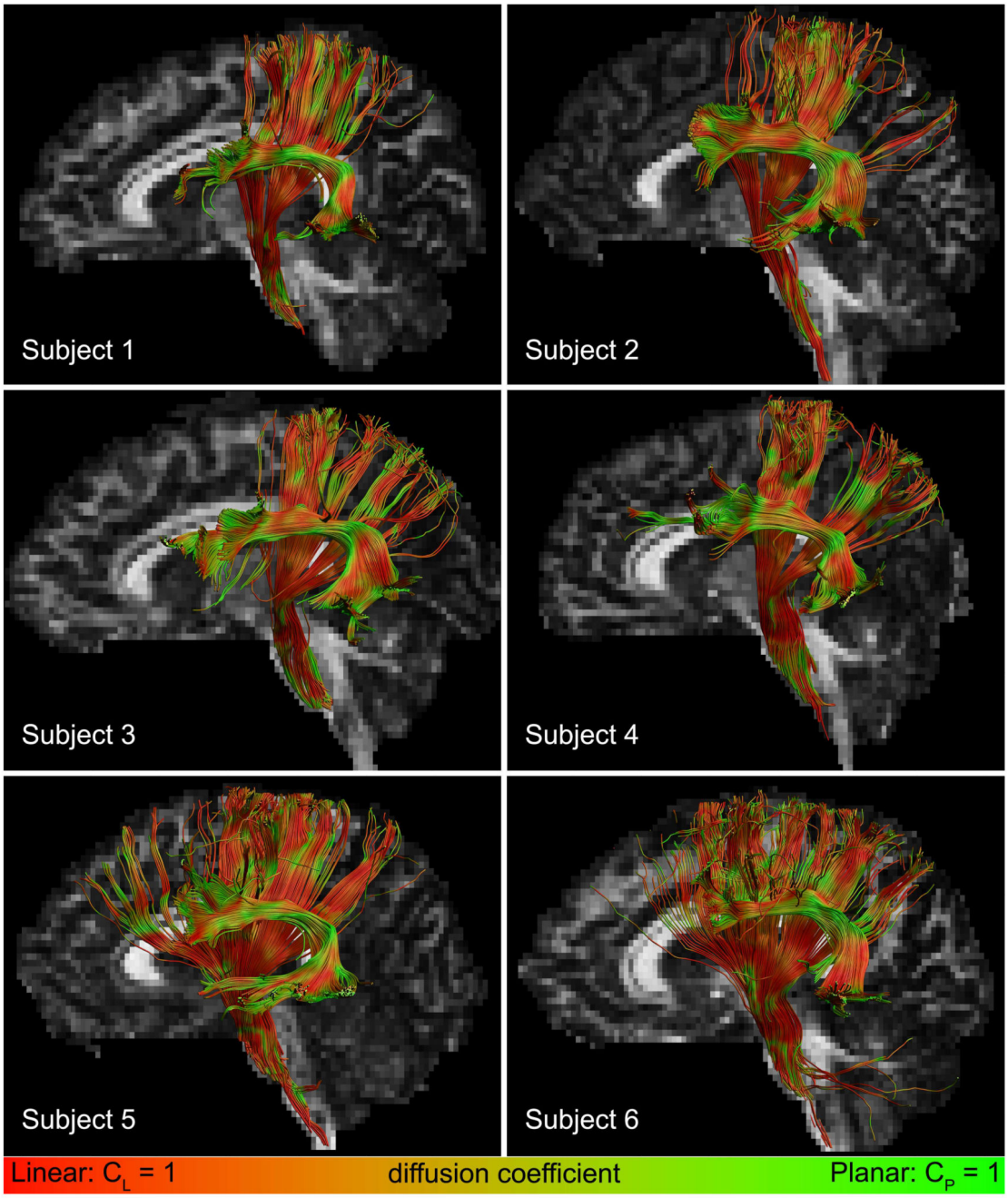

Figure 7.

Sagittal views of a fractional anisotropy map with the cortico-spinal tracts and arcuate fasciculus for all six subjects. Tracts are color-encoded by the linear and planar diffusion coefficients (C_L and C_P, respectively), where red indicates linear diffusion and green indicates planar diffusion.

Europe PMC Funders Author Manuscripts

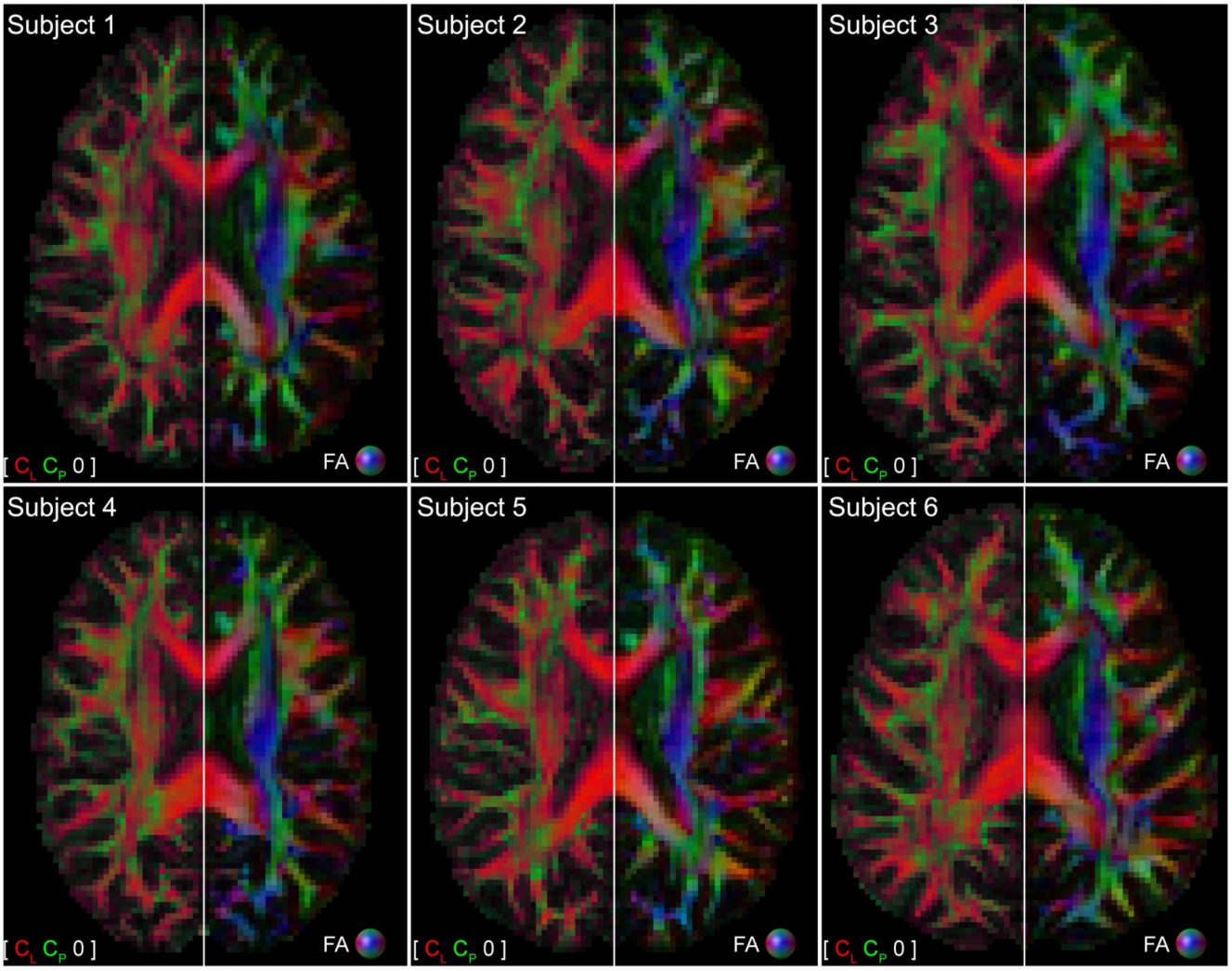

Figure 8.

For all subjects, axial slices at the level of the corpus callosum are shown with geometric and direction-encoded color coding. In the geometric image, red and green voxels correspond with the linear (C_L) and planar (C_P) diffusion coefficients, respectively. Regions of linear and planar diffusion can clearly be differentiated throughout the white matter.

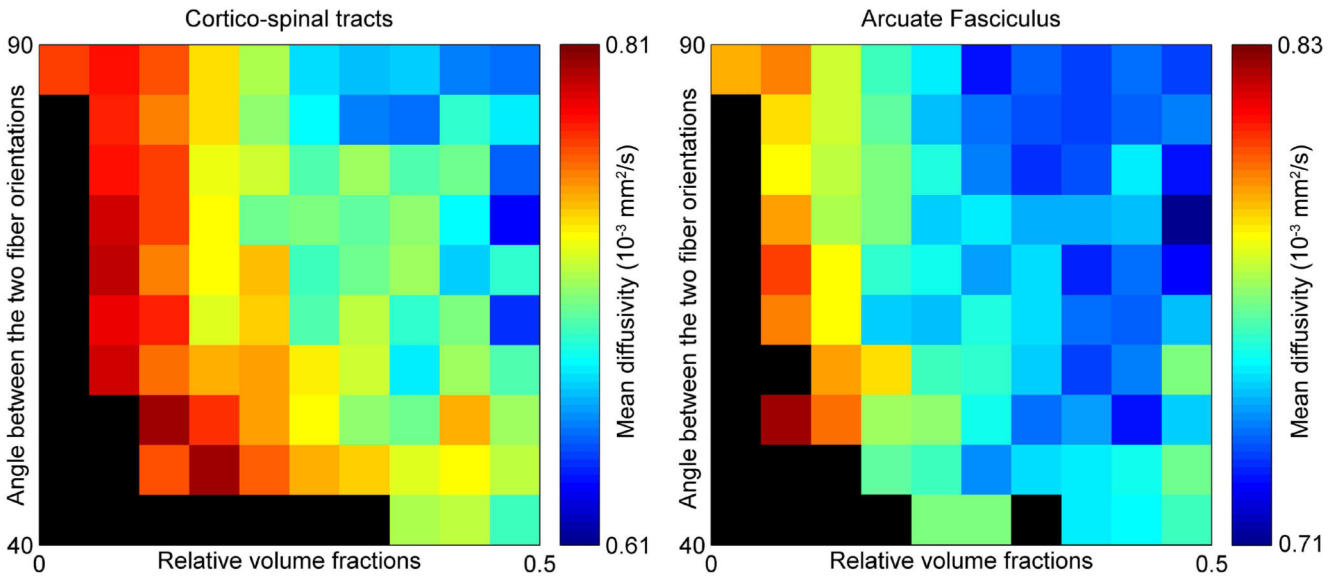

Figure 9.

The mean diffusivity (trace/3) is affected by configurational properties of the white matter. The mean diffusivity decreases as the angle between two fiber populations increases, and the relative volume fractions become more equal. The angles between two fiber populations, as well as the relative volume fractions of these populations, have been determined from constrained spherical deconvolution. The black regions are configurations that were not present.

Table 1

Mean diffusivity values of "single fiber" and "crossing fibers" voxels (in 10^{-3} mm^2/s)

	Cortico-spinal tracts		Arcuate fasciculus		Global white matter	
Subject	**MD^{SF}**	**MD^{CF}**	**MD^{SF}**	**MD^{CF}**	**MD^{SF}**	**MD^{CF}**
1 (female)	0.80 ± 0.09	0.74 ± 0.05 *	0.81 ± 0.07	0.79 ± 0.05 *	0.80 ± 0.07	0.76 ± 0.06 *
2 (male)	0.77 ± 0.08	0.71 ± 0.06 *	0.78 ± 0.08	0.75 ± 0.04 *	0.77 ± 0.07	0.73 ± 0.06 *
3 (male)	0.81 ± 0.10	0.73 ± 0.07 *	0.79 ± 0.07	0.77 ± 0.05 *	0.79 ± 0.08	0.74 ± 0.06 *
4 (female)	0.78 ± 0.11	0.70 ± 0.05 *	0.78 ± 0.06	0.75 ± 0.04 *	0.77 ± 0.07	0.73 ± 0.05 *
5 (female)	0.75 ± 0.09	0.70 ± 0.05 *	0.74 ± 0.06	0.72 ± 0.04 *	0.73 ± 0.07	0.69 ± 0.06 *
6 (male)	0.74 ± 0.10	0.70 ± 0.06 *	0.76 ± 0.08	0.72 ± 0.05 *	0.75 ± 0.08	0.71 ± 0.06 *

Values shown in this table are mean diffusivity values (trace/3), for easy reference with values reported in literature

MD^{SF} is the mean diffusivity (trace/3) in "single fiber" voxels

MD^{CF} is the mean diffusivity (trace/3) in "crossing fibers" voxels

* $p < 0.001$ intra-subject comparison of MD^{SF} *vs.* MD^{CF}